2014 IEEE International Conference on Robotics & Automation (ICRA)
Hong Kong Convention and Exhibition Center
May 31 - June 7, 2014. Hong Kong, China

Terrain Identification on a One-Legged Hopping Robot using High-Resolution Pressure Images

Jacob J. Shill[a], Emmanuel G. Collins, Jr.[a], Eric Coyle[b], and Jonathan Clark[c]
[a]Center for Intelligent Systems, Control, and Robotics (CISCOR)
[c]Scansorial and Terrestrial Robotics and Integrated Design Lab (STRIDe)
[a,c]Department of Mechanical Engineering, FAMU & FSU College of Engineering, Tallahassee, FL, USA
[b]Department of Mechanical Engineering, Embry-Riddle Aeron University, Daytona Beach, FL, USA
jjs05e@my.fsu.edu, ecollins@eng.fsu.edu, coylee1@erau.edu, jeclark@fsu.edu

***Abstract*— For efficient and safe locomotion the gaits of legged robots should vary with the type of terrain. Hence, terrain surface classification is an important problem for this class of mobile robots. Prior research has developed approaches to proprioceptive terrain classification for both wheeled and limbed robots that use sensor measurements dependent upon the dynamics of the robot, which ultimately requires the classification system to be trained at a large number of operating conditions (e.g., vehicle speeds and loads). This research develops an approach to terrain identification based on pressure images generated through direct surface contact using a robot skin constructed around a high-resolution pressure sensing array. Terrain signatures for classification are formulated from the magnitude frequency responses of the pressure images. The methodology is used to train and test a classifier using dynamically measured pressure images from a one-legged hopping robot. Experimental tests yield high classification accuracies, which are independent with respect to changing robot dynamics (i.e., different leg gaits). The findings of this paper suggest the methodology can be extended to autonomous field robots, providing the robot with crucial information about the environment that can be used to aid stability over rough terrains and enhance motion planning over varying terrains.**

I. INTRODUCTION

A robot's locomotion stability and operating efficiency depend on the device's control strategy, leg gait, and the operating environment. Previous research with legged robots has developed a variety of stable leg gaits [1], [2], [3]. A robot's performance however, can be heavily dependent on the type of terrain the robot is traversing [4], [5]. As a result of this terrain dependence, it is important to develop methodologies that enable a limbed robot to recognize new terrain surfaces as they are encountered.

Proprioceptive terrain classification has been accomplished in wheeled vehicles and electric powered wheelchairs primarily by using vibration sensors [6], [7], [8]. For AQUA, a RHex-type legged robot, proprioceptive classification has been performed by using robot leg angles and corresponding leg motor driving currents [9]. Even more recently, the leg motor currents in conjunction with dynamic models for the X-RHex Lite (XRL) robot have been used for surface identification [10]. However, a limitation of each of the above proprioceptive classification methods is that the terrain signatures used for classification are heavily dependent on the vehicle operating conditions such as the speed and load since the measurements are a function of the vehicle's vibration dynamics. (This is discussed in some detail for wheeled robots in [11].) Hence, robust terrain classification requires training for a wide variety of operating conditions, which is a time consuming process and increases classification computational times.

This paper introduces a new proprioceptive method for terrain identification on limbed robots that is largely independent of the vehicle operating condition since it uses sensors that come into direct intermittent contact with the terrain surface. Based on a model of human skin, a robot skin is constructed using a high-resolution pressure sensing array. This robot skin is called Pressure Sensitive Robot Skin (PreSRS, pronounced "pressures"). A classification methodology is developed using the magnitude spatial frequency response of the pressure images obtained using PreSRS. An experiment applying PreSRS to a one-legged robot, the FAMU-FSU Hopper, demonstrates high classification accuracy can be achieved on four common terrain types.

The paper is organized as follows: Section II details how biological inspiration dictated the methodology used to design PreSRS. Section III describes how PreSRS was integrated onto the FAMU-FSU Hopper. Section IV presents the results from dynamic terrain classification experiments on the hopping robot. The results provide strong evidence that the classification approach based on PreSRS images is not dependent upon the vehicle's operating conditions (e.g., leg gait). Section V concludes the paper and presents future work.

II. PRESRS: PRESSURE SENSITIVE ROBOT SKIN

Touch is mediated in human skin using four types of nerve receptors named *Merkel*, *Ruffini*, *Pacini*, and *Meissner* [12]. Nerve ending clusters respond to static and dynamic skin deformation events by sending the form, texture, location, and/or pressure intensity information of the contacting surface to the brain [13]. These qualities of human skin inspired the development of PreSRS using a high-resolution pressure sensing array, the TekScan® #5051 sensor.

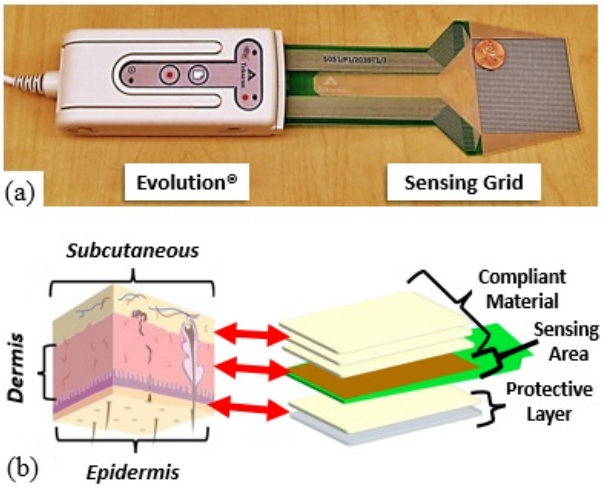

Fig. 1. (a) The TekScan® high-resolution #5051 pressure sensing array attached to the Evolution® data acquisition device [14]. A penny placed on the sensing array provides a size reference. (b) A schematic of PreSRS referencing its multiple layers of compliant material to human skin layers, which posses similar mechanical properties.

The sensing array, shown in Fig. 1(a), consists of 1936 individual piezoelectric based pressure sensors, evenly arranged in a 44 sensor $\times$ 44 sensor grid. The sensing array effectively measures pressure distribution across a 55.88 mm $\times$ 55.88 mm area within a 0-138 kPa range. Sensor readings are acquisitioned with the Evolution® device, also displayed in Fig. 1(a), at a 100 Hz sampling rate [14]. Measurements are saved as 8-bit 44 pixel $\times$ 44 pixel images $\mathbf{I}$, and $\mathbf{I}(i, j)$ represents the pixel corresponding to the individual sensor with grid indexes (i, j).

Human skin consists of the three layers displayed in Fig. 1(b): the (lower) *subcutaneous* layer, the (middle) *dermis* layer, and the (outer) *epidermis* layer.

As illustrated with the PreSRS schematic in Fig. 1(b), the subcutaneous and epidermis skin layers were emulated using sheets of compliant material (each $>$3 mm thick). Human skin is a non-homogenous viscoelastic material, possessing mechanical properties that vary between individuals and skin location [15], [16]. The subcutaneous layer has a desired compliant property of conforming the skin to surfaces, allowing many nerve endings to make contact. A felt type material was found to have this property.

Fig. 1(b) correlates the high-resolution sensing array to the dermis layer of human skin where the nerve receptors reside. The sensor pitch value of 1.27 mm (i.e., the distance between sensors) closely matches human nerve pitch (i.e., the distance between nerves), which can be approximately 1.00 mm in finger tips [17].

The protective nature of the epidermal human skin layer was replicated with a hard silicon-rubber covering ($>$1 mm thick), as shown in Fig. 1(b). The silicon-rubber material has a high stiffness; therefore it deforms negligibly under compression and is resistant to puncture damage.

Altogether, PreSRS is approximately 10 mm thick. Each PreSRS layer was bonded together with 3M™ Super 77 spray adhesive.

III. PreSRS on a One-Legged Hopping Robot

Fig. 2(a) displays the FAMU-FSU Hopper, which can be modeled as a Spring Loaded-Inverted Pendulum (SLIP). The robot has two operating phases, as illustrated in Fig. 2(b): a stance phase, in which the hopper is in contact with a surface, and a flight phase [18].

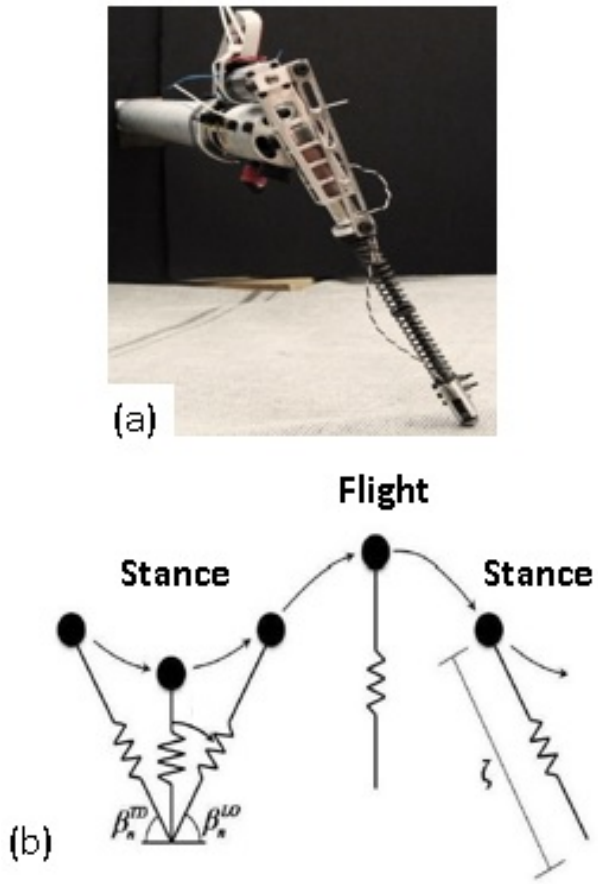

Fig. 2. (a) The one-legged hopping robot, the FAMU-FSU Hopper, used with PreSRS. (b) Illustration of the robot's stance and flight phases.

Stance phase control uses an Active Energy Removal (AER) protocol that changes the robot leg length during a stance as described by,

$$\zeta(t) = \zeta_o - \zeta_{dev} \sin(\omega t + \phi), \tag{1}$$

where ζ_o corresponds to the robot rest leg length, ζ_{dev} depicts the amplitude of recirculation, and the two control parameters ω and ϕ set the desired frequency and phase of recirculation, respectfully. The AER protocol was designed to allow the hopper to robustly run over large obstacles (up to 20% of the robot leg length) [4].

During the flight phase, the controller sets the next robot leg touchdown angle β_{n+1}^{TD} using the governing equation,

$$\beta_{n+1}^{TD} = \beta_n^{LO} + c(\beta_n^{TD} - \beta_{des}^{TD}), \tag{2}$$

where β_n^{TD} is the previous leg touchdown angle, β_n^{LO} is the previous leg liftoff angle, c is a weighted parameter, and β_{des}^{TD} is the desired touchdown angle.

The four control parameters ω, ϕ, c, and β_{des}^{TD} mandate leg gaits $G_i(\omega, \phi, c, \beta_{des}^{TD})$. Parameters ϕ and c are stabilizing factors, and parameters ω and β_{des}^{TD} institute the robot's forward velocity and hop height [4], [18].

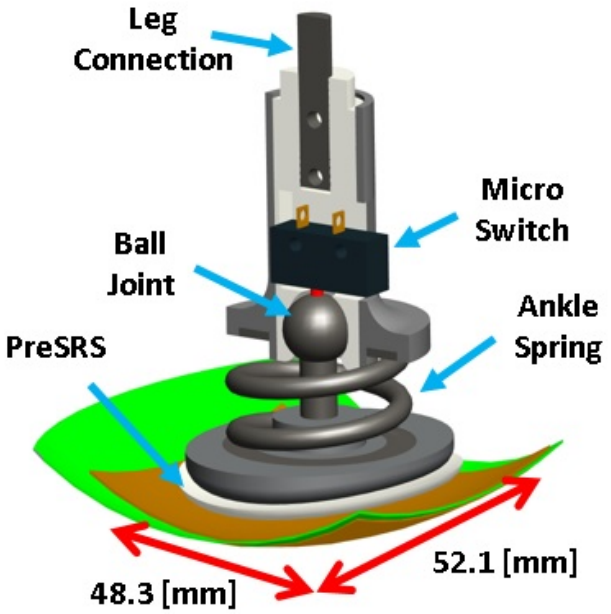

Fig. 3. A sectioned and labeled CAD model of the biologically inspired foot built to accommodate PreSRS on the FAMU-FSU Hopper.

The surface area of the original hopper foot was too small to accommodate PreSRS, which has a 55.88 mm × 55.88 mm sensing area (44 pixel × 44 pixel). Hence, a new robot foot was designed featuring an elliptical base with cross-sectional dimensions of 48.3 mm × 52.1 mm (38 pixel × 41 pixel), as illustrated in Fig. 3. Taking design cues from human ankle biology, enables this new foot to capture consistent high-quality pressure measurements.

The human ankle allows the foot to remain stationary relative to the ground during a step; compressing the viscoelastic adipose tissue beneath the heel, dissipating energy and shock, and conforming the skin to the contacting surface [19], [20]. These biological qualities are replicated with a mechanically compliant ball joint connecting the foot to the hopper leg. Mechanical compliance is governed with the compression spring of Fig. 3. The connection allows the foot to pitch, yaw, and roll as the robot leg progresses through a step. The compliant layers composing PreSRS, shown in Fig. 1(b), compress at impact, which both absorb impact shock and maximize the contact area between the high-resolution pressure array and terrain.

Both the ankle and skin compliances contribute to the dynamic behavior exhibited by the hopper foot during a step, as illustrated in Fig. 4 with high-speed frame shots. As seen in Fig. 4, the foot base flattens, conforming to the surface, and remains stationary relative to the ground over the entirety

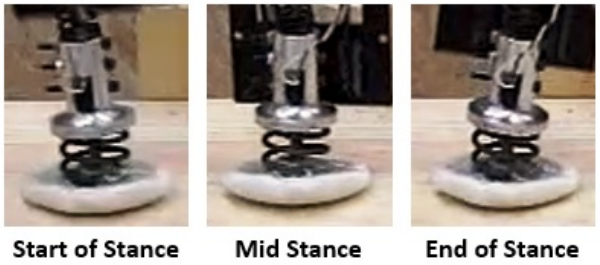

Fig. 4. High-speed video frame shots of the newly designed hopper foot; (Start of Stance) immediately after impacting a surface; (Mid Stance) half way through a step; (End of Stance) the instant before the foot looses contact with the surface.

of the step period, as the robot leg pivots about the ball joint of Fig. 3 from touchdown angle β_n^{TD} to liftoff angle β_n^{LO}.

IV. TERRAIN CLASSIFICATION

Previous terrain classification techniques that use data influenced by the robot dynamics have shown to be effective (achieving accuracies above 90%), so long as the robot operates in the same manner (i.e., leg gait G_i) that is used to train the classifier [8], [9], [10]. Changing operating modes, however, changes the dynamic behavior of the robot, which changes the terrain sensor data. As a result, classifiers for these systems have to be trained with data from multiple operating conditions.

A key motivation for developing PreSRS was to accurately identify terrains regardless of the system operating conditions. PreSRS was designed to capture terrain features through direct contact and not via the robot dynamics. Therefore, a classifier trained with pressure images associated with hopper leg gait G_i should accurately identify terrain samples collected from gait G_j, where $i \neq j$.

It follows from the discussion in Section III, that for fixed stabilizing factors ϕ and c, a hopper leg gait $G_i(\omega, \phi, c, \beta_{des}^{TD})$ can be defined with the two control parameters ω and β_{des}^{TD}. Three distinct leg gaits were used in this experiment, G_1(6.0 rad/sec, 0.27 rad), G_2(6.5 rad/sec, 0.42 rad), and G_3(7.0 rad/sec, 0.57 rad); each successive gait differed by increasing the control parameters ω and β_{des}^{TD}.

Dynamic pressure images were collected using PreSRS and the FAMU-FSU Hopper on four terrain types: smooth pine wood planks, standard flooring carpet, semi-moist clay dirt, and thick Spanish style grass. The circular (2.8 m diameter) track housed the terrains with barriers around the inside and outside perimeter.

Table I displays the average forward velocity of the robot per leg gait G_i on each tested terrain. It should be noted that the robot operated at a greater speed on the grass terrain when compared to the velocities seen on the three other tested terrain types. The compliant nature of the grass used in this experiment may have tuned the hopper effective leg stiffness. Related research has shown that tuning leg stiffness on a RHex type robot can improve locomotion performance [21]. The variant forward velocities between terrains, shown in Table I, underscores the importance of a robot knowing

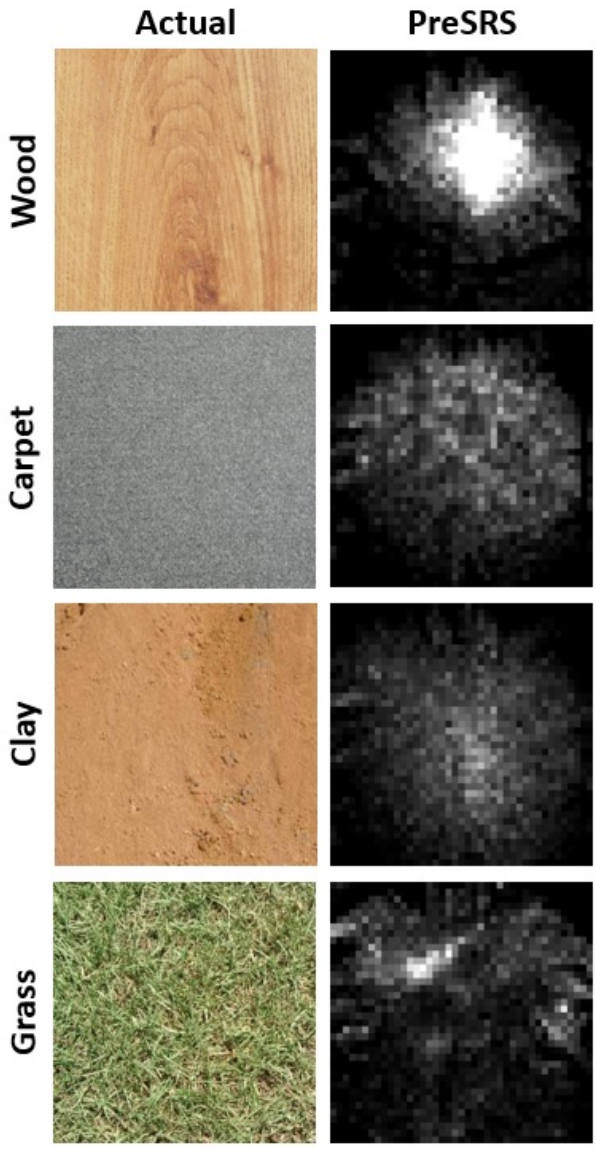

Fig. 5. Example pressure images for each test terrain captured with PreSRS on the FAMU-FSU Hopper. The images contain 38 pixels × 41 pixels, which correlates to a 48.3 mm × 52.1 mm sensing area.

the terrain so that the leg gait parameters can be adjusted accordingly.

TABLE I
HOPPER FORWARD VELOCITIES

	Average Velocities [m/sec]			
Gait	Wood	Carpet	Clay	Grass
G_1	0.40	0.43	0.38	0.81
G_2	0.64	0.63	0.61	1.11
G_3	0.99	0.97	0.84	1.49

The multiple images per terrain type and per leg gait recorded with PreSRS were allocated into three data sets $\mathbf{S}_1$, $\mathbf{S}_2$, and $\mathbf{S}_3$, corresponding to hopper leg gaits G_1, G_2, and G_3, respectfully. Over 300 pressure images $\mathbf{I}$ were collected per leg gait G_i, for a total of 961 images. The bottom 6 rows and first 3 columns of image sets $\mathbf{S}_1$, $\mathbf{S}_2$, and $\mathbf{S}_3$ were cropped to fit the new hopper foot dimensions 48.3 mm × 52.1 mm or 38 pixels × 41 pixels, corresponding to 1558 individual sensors.

Examples of pressure images for each terrain type, taken when the robot was operating with leg gait G_2 are shown in the second column of Fig. 5 in grayscale, where brighter pixels depict higher intensity values. As shown in Fig. 5, the fact that terrain samples captured using PreSRS can be visually distinguished, suggest strong evidence that a high accuracy classifier can be developed.

The Evolution® acquisition device, displayed in Fig. 1(a), records sensor data at 100 Hz. The stance time (i.e., the amount of time the hopper keeps contact with a surface) was approximately 140 msec for each leg gait G_i. The classification results described in this section were obtained by using the middle (i.e., the 7^{th}) recorded pressure image for classification purposes.

It has been shown in [8], [22] that the magnitude frequency response of the spatial domain terrain sample constitutes signatures unique to the terrain type. Hence, it can be used to define feature vectors for use with a classifier.

Feature vectors sets $\mathbf{F}_1$, $\mathbf{F}_2$ and $\mathbf{F}_3 \in \mathbb{R}^n$, where $n = 1025$, corresponding to terrain data collected at each leg gait G_1, G_2, and G_3 respectively, are computed as follows: The rows of the 2D pressure images $\mathbf{I}$ are first aligned and padded with zeroes to obtain $\mathbf{X} \in \mathbb{R}^N$, such that

$$\mathbf{X} = \text{vec}(\mathbf{I}), \tag{3}$$

where $\text{vec}(\cdot)$ is the standard row algining operator, and $N = 2048$. The Fast Fourier Transform (FFT) is used to compute the (spatial) Discrete Fourier Transform $\mathbf{Y} \in \mathbb{C}^N$, given by

$$\begin{aligned} \mathbf{Y}(k+1) &= \sum_{\ell=0}^{N-1} \mathbf{X}(\ell+1) e^{-j2\pi k\ell/N}, \\ k &= 0, 1, \ldots, N-1, \end{aligned} \tag{4}$$

where $\mathbf{Y}(i)$ denotes the i^{th} element of the vector $\mathbf{Y}$. Next, let $\mathbf{Z} \in \mathbb{R}^N$ denote the vector containing the magnitudes of the elements of $\mathbf{Y}$ such that

$$\mathbf{Z}(i) = \text{abs}(\mathbf{Y}(i)), \quad i = 1, 2, \ldots, N. \tag{5}$$

Since the elements of $\mathbf{Z}$ are mirrored, only the first half of the elements are placed in a feature vector $\mathbf{F} \in \mathbb{R}^n$, where $n = N/2 + 1 = 1025$.

Example magnitude frequency responses (i.e., feature vectors $\mathbf{F}_i$) on the each tested surface type are shown in Fig. 6. A key characteristic shared by feature vectors $\mathbf{F}_1$, $\mathbf{F}_2$, and $\mathbf{F}_3$ in Fig. 6, is that in each plot the magnitude spikes occur at the same frequency intervals (48.3 cycle/mm) but with different intensities on each terrain. This frequency interval is an artifact of the piecewise row aligning operation of (3). Spike magnitude differences between terrain types create distinguishing metrics for a classifier to identify.

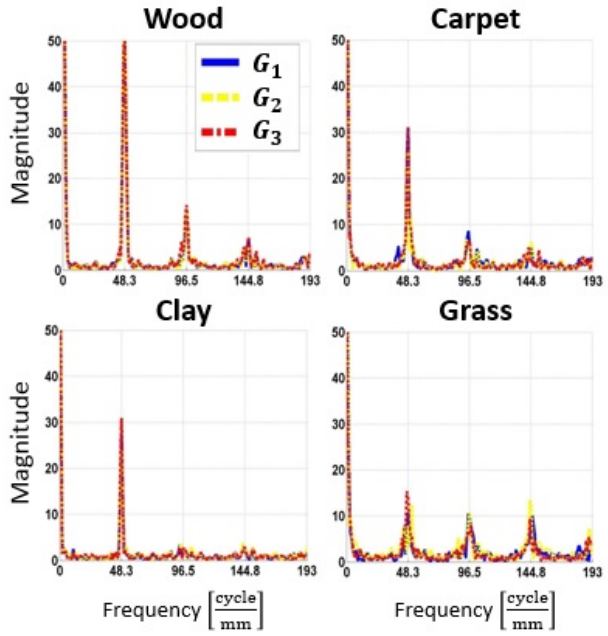

Fig. 6. Sample magnitude frequency response feature vectors $\mathbf{F}_i \in \mathbb{R}^n$, where $n = 1025$, for each of the four tested terrains. Each of the plots contains the three feature vectors $\mathbf{F}_1$, $\mathbf{F}_2$, and $\mathbf{F}_3$ corresponding to leg gaits G_1, G_2, and G_3 for comparison.

Another aspect of Fig. 6, is that the plots seem to contain only one feature vector signature; in fact there are three separate feature signatures in each plot correlating to $\mathbf{F}_1$, $\mathbf{F}_2$, and $\mathbf{F}_3$, respectfully. The feature vectors for each terrain type, show almost indistinguishable profiles. These finding indicate that the pressure based terrain signatures, captured using PreSRS, are indifferent to changes in robot leg gaits.

A Parzen Windows Estimation (PWE) classifier, which is described in [23] in the context of terrain classification, was trained with 20 randomly selected feature vectors, per terrain type (80 total), from set $\mathbf{F}_2$. The 20 feature vectors were split into two sets: 13 for a training set $\mathbf{T} \in \mathbb{R}^{p \times n}$, where $p = 52$, and 7 for a validation set $\mathbf{V} \in \mathbb{R}^{q \times n}$, where $q = 28$.

Principal Component Analysis (PCA) was applied during training to determine a reduced feature space h; this process is discussed in [23]. Using PCA to train the PWE classifier reduces the feature dimensions from $n = 1025$ to $h = 51$. As a result, terrain identification computation times are approximately 0.245 msec when implemented on a 2.67 GHz Intel® Core™2 Duo CPU. Training produces a transformation matrix $\mathbf{U} \in \mathbb{R}^{h \times n}$ for reducing the input feature vector space and a matrix $\mathbf{P} \in \mathbb{R}^{h \times (p+q)}$ that has columns that are reduced order feature vectors resulting from the training.

The surface classification accuracies achieved on the FAMU-FSU Hopper are displayed in Table II. The trained PWE classifier was used to identify feature vectors $\mathbf{F}_1$, $\mathbf{F}_2 \notin \mathbf{P}$, and $\mathbf{F}_3$ by first reducing the order to $\mathbf{Q} \in \mathbb{R}^h$ using $\mathbf{Q} = \mathbf{UF}$. Then the PWE compares $\mathbf{Q}$ with the columns of $\mathbf{P}$ and provides the terrain type most associated with the sample.

As a result, the PWE classifier identified pressure images from each robot leg gait with accuracies over 98% (the highest accuracy being 99.3%). The last row in Table II displays the overall (e.g., average) classification accuracy of the PWE classifier (i.e., the accuracy of identifying 861 terrain samples). Although the results are not displayed in this paper, the PWE classifier produced similar accuracies when trained with terrain samples collected at gaits G_1 and G_3. The identification attributes of the PWE classifier trained at gait G_2, the intermittent gait, displayed the best results.

TABLE II
CLASSIFICATION ACCURACIES

Tested Gait	Accuracy
G_1	99.3%
G_2	99.1%
G_3	98.6%
Overall	99.0%

These findings insinuate that a PWE classifier trained with 20 pressure images, per terrain type using any leg gait G_i produces near perfect identification accuracies when identifying terrains from any leg gait G_j, where $i \neq j$. Hence, PreSRS demonstrates the desired quality of capturing terrain signatures independent of the robot dynamics.

Although not detailed in the paper, additional experiments have shown that the classification procedure is also load independent. Due to the nature of the sensing array whose output is proportional to the applied load, the effects of a change in load from the load during training can be accommodated by simply using a scaling factor. This method holds if the training load is known and the modified load of the vehicle is also known.

V. CONCLUSION

This paper describes the development and demonstration of a proprioceptive approach to surface classification that relies on high-resolution pressure images measured with a robot skin, called Pressure Sensitive Robot Skin (PreSRS). PreSRS was constructed using human skin as a template. The dermis layer consisted of a high-resolution pressure sensing array, which has a pressure sensor density similar to that of human skin. The compliant nature of human skin was replicated using a felt type fabric, which emulates the subcutaneous and epidermis layers. An outer layer of hard silicon-rubber protected PreSRS against puncturing or tearing.

A robot foot was developed for the FAMU-FSU Hopper, enabling the robot skin to have maximal contact with the terrain surface during the stance phases of motion. For a given gait, surface classification was accomplished by extracting pressure images for training and classification at a fixed stance time (i.e., the time after the foot initially impacts the ground). This proved to be highly effective.

Gait-independent terrain classification was demonstrated using the one-legged robot on four distinct terrains, operating under three leg gaits G_1, G_2, and G_3 of increasing velocity. Even though the PWE classifier was trained with data only from the intermediate gait G_2, it was able to identify pressure images recorded at all leg gaits, achieving a near perfect (99.0%) overall accuracy. This approach enables tremendous simplification of the training process in comparison to existing proprioceptive approaches since the classifier requires terrain measurements from just one operating condition, instead of many.

The surface classification approach is based on the observation from [8], [11] that the magnitude of the spatial frequency response of a surface constitutes a terrain signature. Principal Component Analysis was used to reduce the feature vector dimensions to achieve fast classification times. The classifier used in this research was a Parzen Windows Estimator (PWE).

However, as discussed in [23], no one classifier tends to have the overall best performance. Hence, two classification algorithms: Maximum Likelihood Estimation (MLE) and Support Vector Machines (SVM), were investigated; in addition to feature vectors derived from: 2D magnitude frequency response and Gray-Level Co-occurrence Matrix (GLCM) texture attributes [24]. All combinations of feature vector and classifier types produced similarly high accuracies and low computational times. 1D magnitude frequency response feature vectors and the PWE classifier were chosen due to these methods being the most practical to implement in regards to online terrain classification, which is one of the next steps for this research.

In the future, this work will enable autonomous running robots to modify their leg gaits in real-time to reflect changes in the environment; improving speed, stability, and efficiency of running in natural settings and enhancing the accuracy of motion planning. In addition, this approach can be applied to help the end effectors of robot manipulators to identify surface types.

VI. ACKNOWLEDGMENTS

This work was supported by the U.S. Army Research Laboratory under the Robotics Collaborative Technology Alliance program, Cooperative Agreement W91NF-0-2-006.

REFERENCES

[1] Raibert and H. Marc, *Legged Robots That Balance*. Cambridge, MA, USA: Massachusetts Institute of Technology, 1986.

[2] U. Saranli, M. Buehler, and D. E. Koditschek, "RHex: A simple and highly mobile hexapod robot," *International Journal of Robotics Research*, vol. 20, no. 7, pp. 616–631, 2001.

[3] U. Asif and J. Iqbal, "An approach to stable walking over uneven terrain using a reflex-based adaptive gait," *Journal of Control Science and Engineering*, 2011.

[4] B. Miller, B. Andrews, and J. Clark, "Improved stability of running over unknown rough terrain via prescribed energy removal," *12th International Symposium on Experimental Robotics*, 2010.

[5] S. Manjanna, G. Dudek, and P. Giguere, "Using gait change for terrain sensing by robots," in *CRV '13: Proceedings of the 2013 International Conference on Computer and Robot Vision*. IEEE Computer Society, May 2013, pp. 16–22.

[6] E. Coyle, E. Collins, E. DuPont, D. Dang, H. Wang, R. Cooper, and G. Grindle, "Vibration-based terrain classification for electric powered wheelchairs," in *In Proceedings of the Fourth IASTED International Conference on Telehealth and Assistive Technologies*, Baltimore, MD, April 16-18 2008, pp. 139–144.

[7] C. C. Ward and K. Iagnemma, "Speed-independent vibration-based terrain classification for passenger vehicles," *Vehicle System Dynamics*, pp. 1–19, 2008.

[8] E. Dupont, E. Collins, E. Coyle, and R. Roberts, "Terrain classification using vibration sensors: Theory and methods," in *Mobile Robots: New Research*. Nova Science Publishers, Inc., 2010.

[9] P. Giguere, G. Dudek, C. Prahacs, and S. Saunderson, "Environment identification for a running robot using inertial and actuator cues," in *Proceedings of the IEEE Conference on Robotics and Automation*, Montreal, Canada, 2011.

[10] C. Ordonez, J. Shill, A. Johnsons, J. Clark, and E. Collins, "Terrain identification for RHex-type robots," in *Proceedings of the SPIE Defense, Security, and Sensing Conference*, Baltimore, MD, April 29 - May 3 2013.

[11] E. DuPont, C. Moore, E. Collins, and E. Coyle, "Frequency response method for online terrain identification in unmanned ground vehicles," *Autonomous Robots*, vol. 24, no. 4, pp. 337–347, May 2008.

[12] A. B. Vallbo and R. S. Johansson, "Properties of cutaneous mechanoreceptors in the human hand related to touch sensation," *Human Neurobiology*, vol. 3, pp. 3–14, 1984.

[13] Thonnard, Y. Bleyenheuft, and J. Louis, "Development of touch," *Scholarpedia*, vol. 4, no. 10, pp. 58–79, 2009.

[14] TekScan. (2013) Sensor map # 5051. 307 West First Street. South Boston, MA. 02127-1309, USA. [Online]. Available: http://www.tekscan.com/5051-pressure-sensor

[15] J. Pereira, J. Mansour, and B. Davis, "Dynamic measurement of the viscoelastic properties of skin," *Journal of Biomechanics*, vol. 24, no. 2, pp. 157–162, 1991.

[16] X. Liang and S. A. Boppart, "Biomechanical properties of in vivo human skin from dynamic optical coherence elastography," in *IEEE Transactions on Biomedical Engineering*, vol. 57, no. 4, April 2010, pp. 953–959.

[17] M. Lee and H. Nicholls, "Review article tactile sensing for mechatronics - a state of the art survey," *Mechatronics*, vol. 9, no. 1, pp. 1 – 31, 1999.

[18] B. Andrews, B. Miller, J. Schmitt, and J. Clark, "Running over unknown rough terrain with a one-legged planar robot," *Bioinspiration & Biomimetics*, vol. 6, pp. 1–15, June 2011.

[19] H. Elftman, "Dynamic structure of the human foot," *Artifical Limbs*, pp. 13–49, 1969.

[20] G. Kolger and M. Shorten, "Plantar pressure distribution during gait in a subject without adipose tissue in the heel and ball of the foot," *Proc. of the 5th Symp. on Footwear Biomechanics,*, December 2001.

[21] K. Galloway, J. Clark, M. Yim, and D. Koditschek, "Experimental investigations into role of passive variable compliant legs for dynamic robotic locomotion," in *IEEE International Conference on Robotics and Automation*, May 2011.

[22] E. Collins and E. Coyle, "Vibration-based terrain classification using surface profile input frequency responses," in *In Proceedings of the IEEE Conference on Robotics and Automation*, Pasadena, CA, May 19-23 2008, pp. 3276–3283.

[23] E. Coyle and E. Collins, "A comparison of classifier performance for vibration-based terrain classification," in *26th Army Science Conference*, Orlando, FL, December 1-4 2008.

[24] R. Gonzalez and R. E. Woods, *Digital Image Processing*. Prentice Hall, 2002.